Faraday Discussions

Feasibility of Achieving Two-Electron K-O2 Batteries

Journal:	*Faraday Discussions*
Manuscript ID	FD-ART-05-2023-000085.R1
Article Type:	Paper
Date Submitted by the Author:	28-Jun-2023
Complete List of Authors:	Qin, Lei; Shenzhen University Ao, Huiling; The Ohio State University College of Arts and Sciences, Department of Chemistry Wu, Yiying; The Ohio State University College of Arts and Sciences, Department of Chemistry

Feasibility of Achieving Two-Electron K-O_2 Batteries

Lei Qin,[a] Huiling Ao[b] and Yiying Wu*[b]

[a] Prof. L. Qin
Institute for Advanced Study (IAS)
Shenzhen University
Shenzhen 518060, (P. R. China)
[b] H. Ao, Prof. Y. Wu
Department of Chemistry and Biochemistry
The Ohio State University
100 West 18th Avenue, Columbus, OH 43210 (USA)
E-mail: wu@chemistry.ohio-state.edu

Abstract

A deep understanding of the oxygen (O_2) reduction and evolution mechanisms is crucial for understanding the metal-O_2 batteries. It becomes evident that the instability of superoxide in the presence of lithium (Li) ions and sodium (Na) ions is the root cause for the poor reversibility and energy efficiency of Li-O_2 and Na-O_2 batteries. A straightforward yet elegant method is stabilizing superoxide with larger potassium (K) ions. Superoxide-based K-O_2 batteries, invented by our group in 2013, are operated based on one-electron redox of O_2/potassium superoxide (KO_2) and highlighted with high energy efficiencies without any electrocatalysts. Nevertheless, limiting the anionic redox to O_2/superoxide affects the capacity output. Therefore, it is attractive to explore the possibility of beyond KO_2 in the K-O_2 batteries, especially if the use of catalysts can still be avoided. In this research, solid KO_2 was used as the condensed O_2 source and pre-dissolved in the dimethyl sulfoxide (DMSO)-based electrolyte. It is encouraging to observe two sets of reversible peaks during the three-electrode cyclic voltammetry scan under an argon atmosphere. One pair of peaks is attributed to the KO_2/potassium peroxide (K_2O_2) interconversion. Such redox is highlighted with superb reversibility and a small overpotential of 239 mV in the absence of explicit electrocatalysts. Notably, it is further revealed that K_2O_2 reacts with gaseous O_2. Therefore, a gas-open system with an O_2 supply is unfavorable for realizing the reversible KO_2/K_2O_2 redox, and a closed cell system with a KO_2 supply as the starting active material is suggested instead.

Introduction

Directly utilizing oxygen (O_2) as the cathode active component offers several attractive benefits: higher specific capacities and inexhaustible O_2 supply from ambient air. The electron is stored based on the lightweight O element with a maximum $4e^-$ per O_2 molecule, offering its high theoretical capacity. In comparison, the conventional lithium-ion cathode materials rely on the redox of much heavier transition metal ions (e.g., Fe^{3+}/Fe^{2+} in $LiFePO_4$). Therefore, research in different metal-O_2 batteries has been actively explored in the field of energy storage community.

As the final O_2 reduction product in aqueous electrolytes, hydroxide formation implies a theoretical 4-electron transfer process ($4e^-$ per O_2 molecule), but it requires essential catalysts to boost the reaction kinetics. Empirically, such the 4-electron transfer process can only be achieved in aqueous media with hydroxide as the final discharge product (e.g., hybrid Na-O_2 battery),[1] because the formation of alkali metal oxide is kinetically/thermodynamically unfavorable in non-aqueous electrolytes. Pioneering research was reported by the Nazar team that utilized an elevated temperature (150 ^oC) to stabilize lithium oxide (Li_2O) as the

primary product in an aprotic Li-O_2 battery system and demonstrated a reversible 4-electron conversion between O_2 and Li_2O by using a nickel-based catalyst in the molten salt electrolyte.[2] Recently, Curtiss and Asadi reported a room-temperature rechargeable Li_2O-based Li-O_2 battery enabled by using a composite polymer electrolyte based on $Li_{10}GeP_2S_{12}$ nanoparticles embedded in a modified polyethylene oxide polymer matrix.[3] The key to realizing the four-electron reaction is to form a mixed ion/electron-conducting discharge product intermediates of superoxide/peroxide and its interface with gas based on their explanation.

Although the one-electron reduction process from O_2 to superoxide is kinetically favorable during discharging the alkali metal-O_2 batteries, the generated superoxide can occur self-disproportionation or further electrochemical reduction to peroxide for Li-O_2 and Na-O_2 systems, which can be ascribed to the superior thermodynamical stability of Li_2O_2 and Na_2O_2 over superoxide counterpart. A recent finding reveals that the chemical disproportionation of unstable superoxide intermediate is the main source for singlet O_2 ($^1O_2$) generation.[4] It becomes clear that the reactive $^1O_2$ easily triggers the electrode/electrolyte degradation, thus greatly deteriorating the battery performance. Moreover, despite more electrons passing per O_2 molecule from superoxide to peroxide as final discharge products, the peroxide batteries ($2e^-$ per O_2 molecule) exhibit high round-trip overpotentials (typically above 1.0 V for Li-O_2 and Na-O_2 batteries). Therefore, active electrocatalysts are essential, especially for improving the sluggish decomposition kinetics of peroxide. The incorporation of extra catalysts into the O_2 cathode would add costs.

Recently, superoxide batteries ($1e^-$ per O_2 molecule) have received tremendous attention given the high reversibility of O anionic redox with facile kinetics. Although sodium superoxide (NaO_2) is the possible discharge product of a Na-O_2 cell,[5] NaO_2 suffers from low shelf-life and converts to hydrated Na_2O_2 spontaneously through electrolyte degradation upon aging.[6] Lithium superoxide (LiO_2) may be stabilized by iridium nanoparticles via a proposed "template-based growth" route based on a recent study,[7] but Li_2O_2 is still the primary discharge product in a conventional Li-O_2 battery. In contrast, potassium superoxide (KO_2) possesses excellent long-term stability and is the sole primary discharge product without the interference of potassium peroxide (K_2O_2) in a K-O_2 battery.[8] Notably, K is the lightest alkali metal element that can form the thermodynamically stable superoxide. Our group invented the K-O_2 battery based on KO_2 formation/decomposition in 2013 (**Figure 1**a).[9] Such the O_2/KO_2 redox is a typical one-electron transfer process ($1e^-$ per O_2 molecule). The KO_2-based K-O_2 battery is highlighted with high reaction kinetics in the absence of electrocatalysts, providing an elegant solution to the kinetic challenges in air cathodes.[10] This is different from the multielectron transfer process in fuel cells, Zn-O_2 ($4e^-$ per O_2 molecule), and Li-O_2 ($2e^-$ per O_2 molecule) batteries that suffer from sluggish reaction kinetics.

Typically, the K-O_2 cell delivers low discharge/charge overpotentials (ca. ~50 mV) at moderate current densities, which enhances the round-trip efficiency ($>$95%) (**Figure 1**b). Notably, the K-O_2 battery is the only alkali metal-O_2 system that does not generate $^1O_2$. The stable product of KO_2 would not occur disproportionation during the discharge/charge processes, and the decomposition of KO_2 is finished below 3.0 V (vs. K^+/K). Under such operation conditions, no $^1O_2$ is evolved, and side reactions associated with electrode/electrolyte decomposition are also alleviated. In addition, our recent study shows that KO_2 is extremely sensitive to moisture but relatively stable in dry CO_2.[11] Given the intrinsic stability of KO_2 in the O_2 and N_2 atmosphere, the O_2/KO_2 redox is unaffected by dry ambient air. Therefore, the K-O_2 has the advantage of operating as a true *air* battery rather than an *O_2*

battery. Only a moisture trap is required to remove moisture before purging ambient air into a K-air (dry) battery. Additionally, KO_2 is the only commercially available superoxide that can be massively produced. As a result, the proof-of-concept of a graphite-KO_2 cell (**Figure 1**c),[12] which represents the fully discharged state, can be assembled with the dry-room manufacturing technique. This could avoid handling the reactive metallic K or potassiated graphite in the full-cell demonstration. Such advantage has seldom been emphasized priorly and would be important in battery manufacturing.

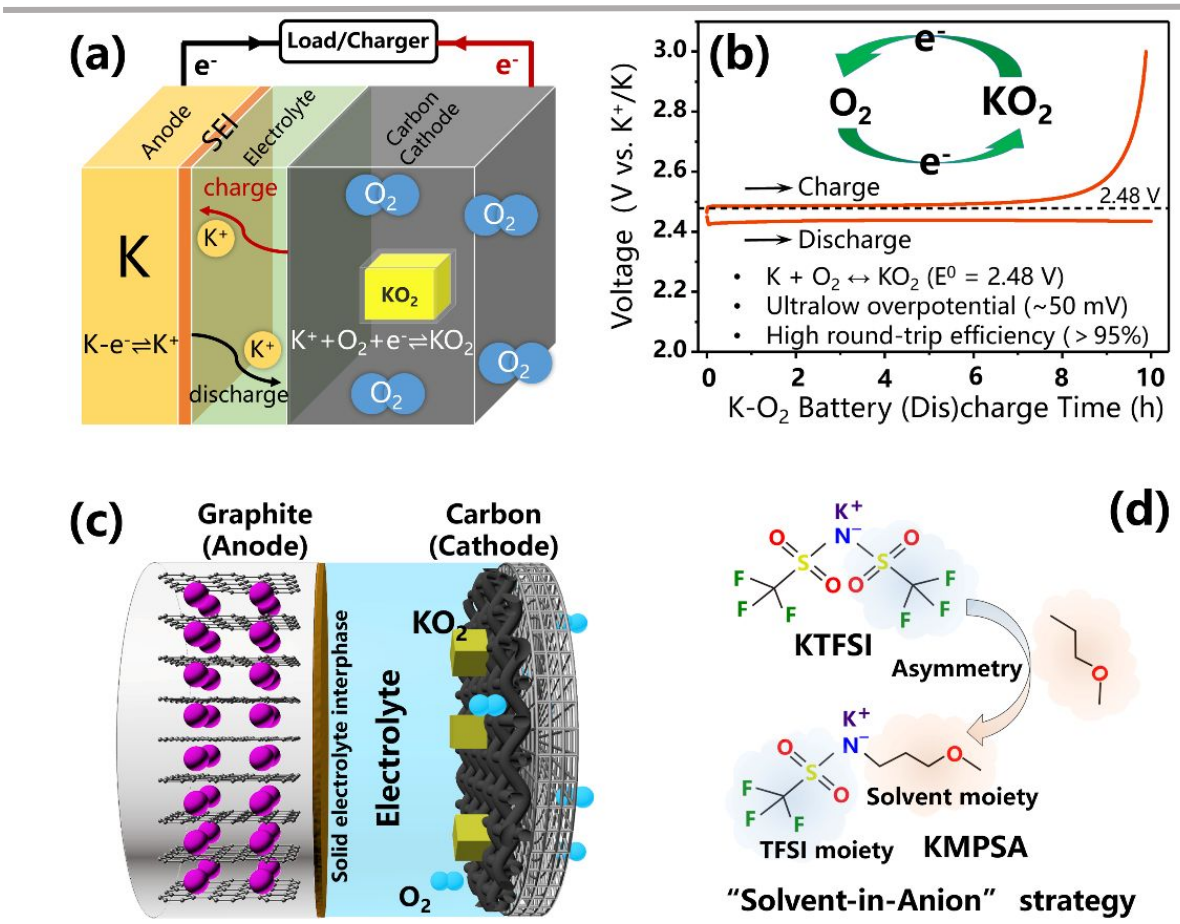

Figure 1. (a) Working principle of a rechargeable K-O_2 battery. (b) Representative voltage profile of a K-O_2 battery based on single-electron O_2/KO_2 redox. (c) The proof-of-concept of a graphite-KO_2 cell. (d) Concept of solvent-in-anion design for asymmetric K salts.

Nevertheless, all the alkali metal-O_2 batteries suffer from several intrinsic drawbacks: a gas-open system using O_2 from ambient air faces intractable issues of air purification, anode deactivation due to O_2 crossover, and evaporation of volatile electrolytes. A closed system connecting to a gas reservoir for O_2 storage would suffer from sacrificing volumetric energy density. Furthermore, despite its superb reaction kinetics, superoxide-based K-O_2 batteries deliver a limited capacity of 377 mAh g^{-1} (based on KO_2 mass). More electrons are stored in the O element when moving from superoxide to peroxide and ultimately oxide, resulting in enhanced capacity output. Moreover, confining the electrochemical conversion between solid-phase superoxide, peroxide, and monoxide can not only inherit the benefits of O-related anionic redox but also avoid the challenges associated with gaseous O_2 participation/evolution. With intensive efforts from many prominent research groups, the proof-of-concept of O-related anion-redox cathodes involving oxide/peroxide, oxide-

peroxide/superoxide, and peroxide/superoxide interconversion have been realized in the lithium-based system, allowing the use of sealed cell configuration. The critical issue for the successful demonstration is to confine Li_2O nanoparticles into an efficient catalyst skeleton (cobalt oxide-carbon black[13] or iridium-graphene composite[14]) or stabilize the formation of amorphous LiO_2 with an explicit palladium-graphene hybrid catalyst.[15]

It is stimulated whether a similar idea can also be applied to the K-O system, especially if the usage of catalysts can be avoided. Lu et al. utilized the ambient pressure photoelectron spectroscopy (APXPS) technique to probe the electrochemistry in K-O_2 electrochemistry and first identified the possible discharge products of K_2O_2 and K_2O at a high depth of discharge.[16] Recently, Haoshen Zhou's group has reported a cathode consisting of nanoscale KO_2 confined in a ruthenium oxide (RuO_2)-reduced graphene oxide substrate, enabling the reversible interconversion between KO_2 and K_2O_2 based on a proposed solid-solid transformation mechanism.[17] However, the use of excessive RuO_2 as the electrocatalyst (30 wt%) dramatically increases the cost. Our group has demonstrated an enhanced KO_2/K_2O_2 conversion by adopting a high-donicity anion additive in the ether-based electrolyte (**Figure 1**d).[18] The anion additive was synthesized via a "Solvent-in-Anion" strategy that could tune the electron donicity of electrolyte salts and thus change the solvation structure of the electrolyte. A significant achievement of using high-donicity anion is to enhance KO_2 utilization (~90.2 %) by retarding electrode passivation and allow the full charging back of K_2O_2 through the solution-mediated pathway in the absence of explicit catalysts. However, the low compatibility of high-donicity anions with K anode remains a critical issue that limits the overall battery lifespan.

Previous studies reported by Baltruschat[19] and Ramani[20] have indicated two sets of noticeable redox peaks in the dimethyl sulfoxide (DMSO)-based electrolyte during three-electrode cyclic voltammograms of O_2 reduction reaction (ORR). The second reduction peak is ascribed to the generation of peroxide species. It is encouraging to observe that K_2O_2 undergoes facile decomposition with a small voltage gap of ~100 mV without any catalysts. Nevertheless, the two-electron O_2/K_2O_2 has yet to be realized in a full-cell configuration.

The representative papers and major achievements abovementioned on Li-O_2, Na-O_2, and K-O_2 batteries system are listed in **Table 1**. In the past, there have been many excellent summaries on Li-O_2 and Na-O_2 batteries based on peroxide chemistry.[21–24] Distinct from the direct two-electron process between the O_2/peroxide, it is reasonable to think that utilizing the anionic redox of O_2/superoxide and superoxide/peroxide couple could be a promising solution to address the kinetics challenges in air cathode. K is the lightest alkali metal that forms stable superoxide. Therefore, a battery based on $O_2/KO_2/K_2O_2$ redox is attractive to explore. This article aims to highlight the unique advantages of superoxide-based K-O_2 chemistry and clarify the importance of "beyond superoxide" prompted by storing more electrons in O_2. We also discuss the current challenges and explain our perspectives on how to utilize the $O_2/KO_2/K_2O_2$ redox in practical batteries.

Table 1. Summary of the representative papers and major achievements on the alkali metal-O_2 systems.

O-related anionic redox	Li-O_2	Na-O_2	K-O_2
O_2 to superoxide	Iridium-rGO composite cathode[7]	Gas-diffusion layer (GDL): carbon paper[5]	GDL[9]
O_2 to peroxide	Conductive GDL in conventional cases	Peroxide from NaO_2 conversion via electrolyte degradation upon aging[6]	APXPS technique with a carbon cathode in ionic liquid-based electrolytes[16]
O_2 to oxide/hydroxide	Ni catalyst in $LiNO_3/KNO_3$ molten salt electrolyte (150 °C)[2]	Bifunctional ORR/OER[a] catalyst-NASICON solid electrolyte based on aqueous catholyte in hybrid Na-O_2[1]	APXPS technique with a carbon cathode in ionic liquid-based electrolytes[16]
	$Li_{10}GeP_2S_{12}$-polyethylene oxide-based composite solid electrolyte[3]		
Superoxide to peroxide	Pd-rGO catalyst[15]	N/A	CV with DMSO-based solvent[19,20]
			High donor-number anion[18]
			RuO_2-rGO-KO_2 composite cathode[17]
Superoxide/peroxide to oxide	Co_3O_4-Li_2O composite cathode[13]	N/A	N/A
	Ir-rGO-Li_2O composite cathode[14]		

Notes: [a] OER is the abbreviation of oxygen evolution reaction.

Results and discussion

To avoid anode interference, the three-electrode setup was adopted to investigate the O-related anionic redox in terms of reversibility and redox polarization. Note that the planar glassy carbon (GC) was used as the working electrode, while the platinum (Pt) wire and $Ag/AgNO_3$ were adopted as the counter and reference electrodes, respectively.

The well-defined two reversible O-related anionic redox peaks in DMSO-based electrolytes

The thermodynamic stability of KO_2 makes it the exclusive superoxide that can be produced massively. Therefore, the solid KO_2 is treated as the condensed O_2 source, allowing the experiments to operate without purging gaseous O_2. This advantage has not been highlighted in previous tests.[19,20] In our designed experiment, the commercial KO_2 powder was directly added into 0.1 M KPF_6/DMSO electrolyte (**Figure 2**). After stirring the suspension overnight in the argon (Ar)-filled glovebox, the suspension was filtrated to remove the insoluble solid. The obtained clear filtrate was denoted as KO_2-saturated electrolyte and then transferred into the four-necked flask for further electrochemical tests.

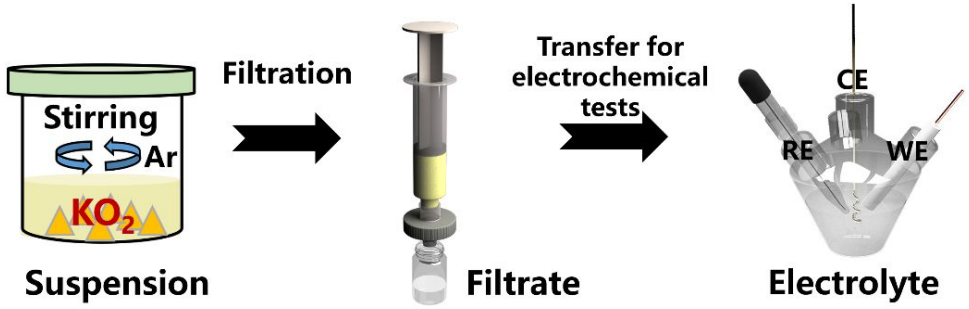

Figure 2. Procedures for preparing the KO_2-saturated 0.1 M KPF_6/DMSO electrolyte for three-electrode cyclic voltammetry (CV) tests. (See the details in the **Experimental Section**).

The two well-defined redox peaks can be observed in the inert Ar atmosphere using the prepared KO_2-saturated electrolyte. The O1/R1 redox occurring at a more positive voltage range is ascribed to O_2/KO_2, while the O2/R2 redox is attributed to KO_2/K_2O_2 (**Figure 3**a). Both redox reactions are highly reversible with small voltage gaps for O1/R1 redox (~109 mV) and O2/R2 redox (~239 mV) at a scan rate of 50 mV s^{-1} (**Table 2**). Such two redox peaks are also noticeable with superb reversibility even at a scan rate of 200 mV s^{-1} (**Figure 3**b).

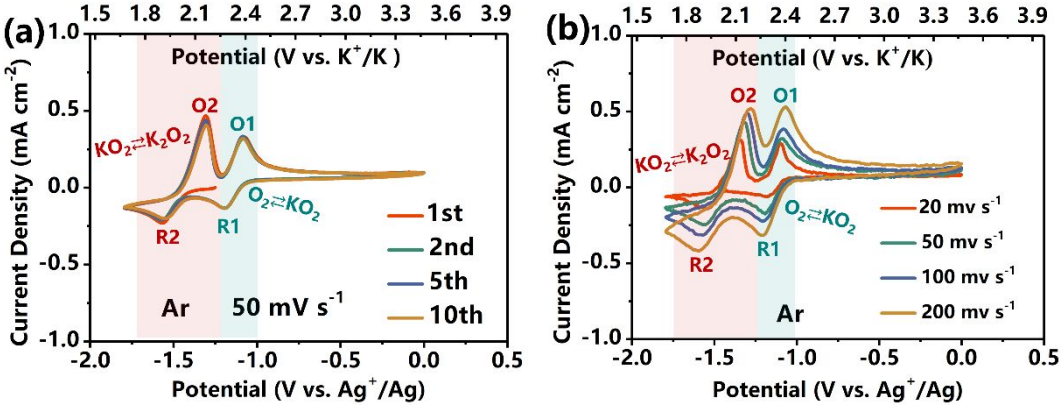

Figure 3. CV scans of a GC electrode under Ar atmosphere. The electrolyte is 0.1 M KPF_6/DMSO saturated with KO_2. (a) The first 10 cycles at a constant scan rate of 50 mV s^{-1}. (b) CV scans at different scan rates. R1 and R2 indicate the formation of KO_2 and K_2O_2, while O1 and O2 denote the decomposition of KO_2 and K_2O_2. The voltage range is set as 0~-1.8 V vs. Ag^+/Ag. 0 $V_{Ag+/Ag} \equiv 3.47$ $V_{K+/K}$ in the DMSO-based electrolyte, and detailed information can be found in the **Experimental Section**.

Table 2. Voltammetric properties of KO_2-saturated 0.1 M KPF_6/DMSO electrolyte at various scan rates. CV curves were collected on the GC electrode in the Ar atmosphere.

Scan rate (mV s^{-1})	$Ep_{(R1)}$ (V)	$Ep_{(O1)}$ (V)	Overpotential (R1/O1) (V)	$Ep_{(R2)}$ (V)	$Ep_{(O2)}$ (V)	Overpotential (R2/O2) (V)
20	-1.185	-1.098	0.087	-1.543	-1.348	0.195
50	-1.190	-1.085	0.105	-1.558	-1.320	0.238
100	-1.203	-1.083	0.120	-1.568	-1.298	0.270
200	-1.208	-1.068	0.140	-1.598	-1.278	0.320

The peak current densities for specific redox peaks can be measured by extrapolating the preceding current baseline (**Figure 4**a). The calculated R^2 values of fitting lines for two reduction (R1 and R2) peaks are very close to 1, implying a good linear relationship between peak current densities and square root of scan rates (**Figure 4**b). Therefore, the electrochemical reduction reactions (R1 and R2) in the DMSO-based system are mainly

controlled by the diffusion of active species rather than by a factor of kinetics. However, prior studies have shown that K_2O_2 is insoluble in DMSO.[25,26] The insoluble K_2O_2 that deposits on the electrode is still rechargeable with high reversibility, as evidenced by relatively small potential gaps even at higher scan rates (**Figure 3**b). The linear relationship for Ip(O2) and $v^{1/2}$ could then arise from diffusion-controlled reduction of soluble KO_2 to K_2O_2 in previous scan, which determines amount of K_2O_2 available for reoxidation. Notably, a discrepancy exists between reduction and oxidation peak current densities (**Table 3**). Moreover, the voltammograms exhibit a larger separation in peak potentials than that (59 mV) of a reversible one-electron redox, implying a quasi-reversible electrochemical process (**Table 2**). Nevertheless, the two single-electron transfer processes are still characteristic of superb reaction kinetics without requiring solid electrocatalysts or liquid redox mediators, which is first reported and achieved in an inert Ar atmosphere.

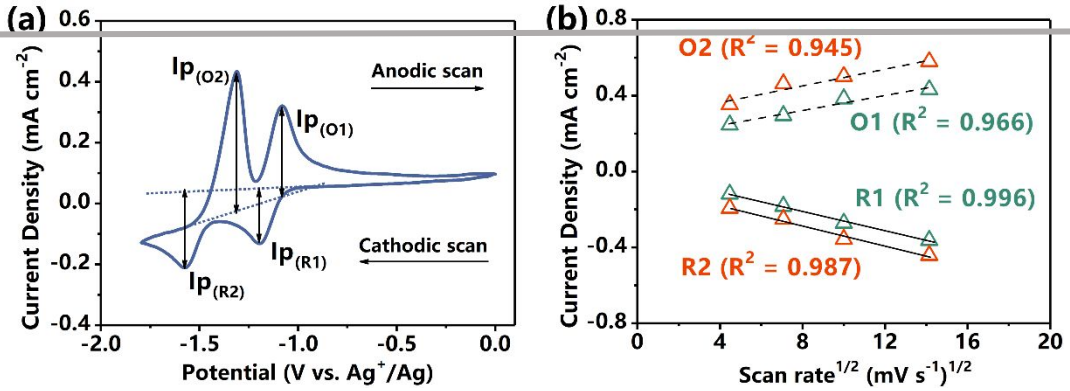

Figure 4. (a) Typical CV of GC electrode in KO_2-saturated 0.1 M KPF_6/DMSO electrolyte at a scan rate of 50 mV s^{-1}. The auxiliary dot lines are added to help estimate the peak current densities of redox peaks. (b) The plot of the square root of CV scan rates versus experimental peak current densities.

Table 3. The peak current densities (I_p) for O_2/KO_2 couple and KO_2/K_2O_2 couple. The R1/O1 peaks are used for O_2/KO_2, and the R2/O2 peaks are used for KO_2/K_2O_2. The raw CV data is from **Figure 3**b.

Scan rate (mV s^{-1})	$Ip_{(R1)}$ (mA cm^{-2})	$Ip_{(O1)}$ (mA cm^{-2})	$Ip_{(R2)}$ (mA cm^{-2})	$Ip_{(O2)}$ (mA cm^{-2})
20	-0.119	0.246	-0.194	0.354
50	-0.183	0.296	-0.251	0.463
100	-0.272	0.384	-0.357	0.502
200	-0.363	0.432	-0.442	0.58

Effect of cation types on the reversibility of O-related anionic redox

CV response for O_2 reduction was collected in the presence of different cations. The unstable nature of superoxide in the presence of Li^+ and Na^+ would result in spontaneous peroxide formation via the self-disproportionation of superoxide. The overall net reaction is from O_2 to peroxide (0 to -2) during the ORR. Notably, the decomposition of peroxides (Li_2O_2 and Na_2O_2) suffers from sluggish reaction kinetics. Such a two-electron transfer process is characteristic of low reversibility with an obvious current decay upon scans and high polarization (~1.65 V for O_2/Li_2O_2 and ~0.64 V for O_2/Na_2O_2) at 50 mV s^{-1} (**Figure 5**). In comparison, the stability of superoxide anion is greatly enhanced when changing the cation from Li^+ or Na^+ to K^+, which can be explained by Pearson's hard-soft acid-base theory[27]. Therefore, two separate one-electron processes (0 to -1 and -1 to -2) can be identified and

observed with high reversibility and reaction kinetics in the K-O system, which provides a simple but elegant solution to address the challenge of peroxide decomposition in O_2 electrodes.

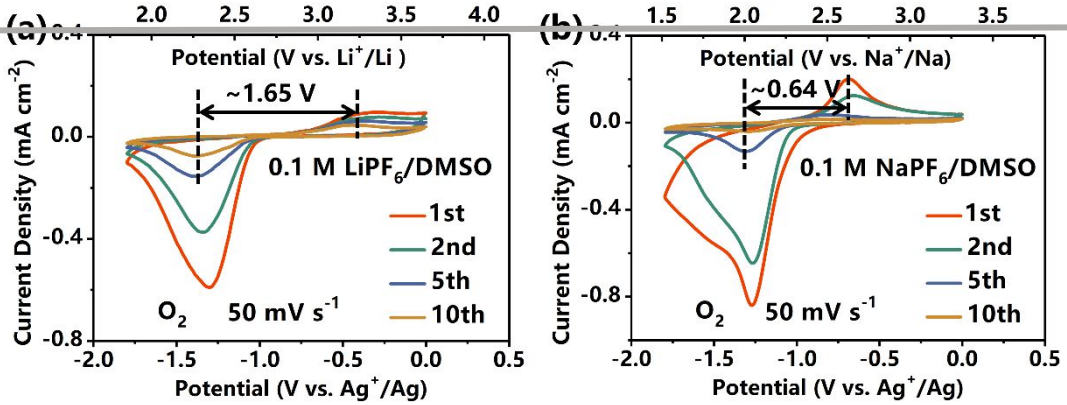

Figure 5. CVs demonstrating the significant effect of cation type on the reversibility of O_2 reduction/evolution reaction. Data was collected on the GC working electrode in O_2-saturated (a) 0.1 M $LiPF_6$/DMSO and (b) 0.1 M $NaPF_6$/DMSO. The scan rate is 50 mV s^{-1}.

Effect of operation atmosphere on the reversibility of $O_2/KO_2/K_2O_2$ redox

When the KO_2-saturated electrolyte is purged with O_2, the peak O2 ($K_2O_2 \rightarrow KO_2$) is absent despite the presence of peak R2 ($KO_2 \rightarrow K_2O_2$) (**Figure 6**a). In addition, the peak O1 attributed to KO_2 decomposition exhibits an ever-increasing polarization upon cycles**.** The redox reversibility was also evaluated with 0.1 M KPF_6/DMSO electrolyte in the O_2 atmosphere (**Figure 6**b). It is observed that the first one-electron transfer process of O_2/KO_2 redox is still reversible. However, the peak O2 attributed to K_2O_2 oxidation ($K_2O_2 \rightarrow KO_2$) gradually decreases in current intensity upon cycles until the complete disappearance at the 20th cycle. It is reasonable to think that the insoluble K_2O_2 that precipitates on the electrode surface could be chemically oxidized to KO_2 by O_2, and therefore induce the disappearance of the peak O2. Compared to the insoluble K_2O_2, the KO_2 with a higher solubility could dissolve into DMSO electrolyte and further be electrochemically decomposed during the positive-going scan, which is evidenced by the nearly unchanged O1 current response (**Figure 6**b). The difference between Figure 6a and 6b is attributed to the saturation of the electrolyte in Figure 6a by KO_2, which results in the precipitation of KO_2 and passivation of the electrode surface.

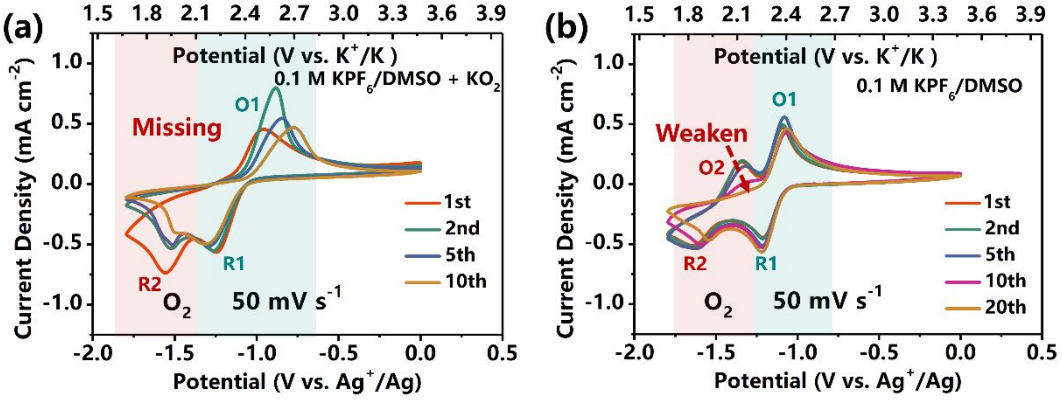

Figure 6. CV scans of a three-electrode setup (working electrode: GC; counter electrode: Pt wire; reference electrode: $Ag/AgNO_3$ in MeCN) in the O_2 atmosphere at a scan rate of 50 mV s^{-1}. The electrolyte is (a) KO_2-saturated 0.1 M KPF_6/DMSO and (b) 0.1 M KPF_6/DMSO.

Chemically synthesize K_2O_2 and its stability evaluation in the O_2 atmosphere

It has been revealed in prior studies that the stability of K_2O_2 and KO_2 strongly depends on the O_2 partial pressure and temperature. In the specific temperature range (0~500 °C), superoxide is the thermodynamically stable phase at a high O_2 partial pressure, while peroxide is more stable at a lower O_2 partial pressure.[28] It is further estimated that K_2O_2 becomes a more thermodynamically stable phase than KO_2 only when the O_2 partial pressure is below 10^{-6} bar at room temperature. Actually, the existing literature on reporting K_2O_2 preparation is via the thermal decomposition of KO_2 at 588 K with the dynamic vacuum (p ~$2.0*10^{-3}$ mbar), which also implies the dependence of K_2O_2 stability on the O_2 partial pressure.[29] To give more direct evidence to support the hypothesis, it is essential to directly synthesize K_2O_2 to study its chemical properties. Herein, two methods were proposed to synthesize K_2O_2 by utilizing the chemical reactions between KO_2 and K or K_2O, respectively (**Figure S1**a-b). Based on the thermodynamic parameters collected from previous reports (**Table 4**), the isothermal relations of Gibbs free energy (Reaction 1 & 2) are listed below:

$$K\ (s) + KO_2\ (s) \rightarrow K_2O_2\ (s);\ \Delta G^0(kJ \cdot mol^{-1}) = -209.2 + 0.0793T \quad \text{(Reaction 1)}$$

$$2K_2O\ (s) + 2KO_2\ (s) \rightarrow 3K_2O_2\ (s);\ \Delta G^0(kJ \cdot mol^{-1}) = -186.2 + 0.11516T \quad \text{(Reaction 2)}$$

Table 4. Thermodynamic parameters for different substances.

Compounds	ΔH_f^0 (kJ/mol)	ΔG_f^0(kJ/mol) at 298K	ΔS(J/mol)
KO_2 (s)	-284.9	-239.4	116.7
K_2O_2 (s)	-494.1	-425.1	102.1
K_2O (s)	-363.17	-322.1	94.03
K (s)	0	-	64.7
O_2 (g)	0	-	205.2

XRD tests were conducted to detect the synthesized products. For the product via **Reaction 1**, it is easy to identify the starting material of KO_2 residue apart from the target product of K_2O_2, which indicates the incomplete reaction (red trace in **Figure S1**c). By utilizing the comproportionation between KO_2 and K_2O solids via **Reaction 2**, it is found that there is only K_2O_2 as the final product without the interference of starting materials residue, as evidenced by its typical XRD pattern (cyan trace in **Figure S1**c) and Raman peak at ~760 cm^{-1} (**Figure S2**a). As shown in typical SEM images, the as-synthesized K_2O_2 particles possess the morphology of secondary aggregates within several micrometer scales (**Figure S2**b). The successful synthesis of pure K_2O_2 allows us to investigate its intrinsic property, such as its stability in O_2. Typically, the as-synthesized K_2O_2 powder was put inside the air-tight vial, which was refilled with a pure O_2 atmosphere (**Figure 7**a). After resting the K_2O_2 sample in O_2 for 70 hours, the aged sample shows a typical color of light yellow, which is distinct from the pristine K_2O_2 with a beige color. In addition, the typical XRD pattern of the aged sample reveals the existence of newborn KO_2 besides parent K_2O_2 (cyan trace in **Figure 7**b). The above observations imply the instability of K_2O_2 in the presence of O_2. The side reaction and the related isothermal relation of Gibbs free energy (Reaction 3) are listed below:

$$K_2O_2\ (s) + O_2\ (g) \rightarrow 2KO_2\ (s);\ \Delta G^0(kJ \cdot mol^{-1}) = -75.7 + 0.0739T \quad \text{(Reaction 3)}$$

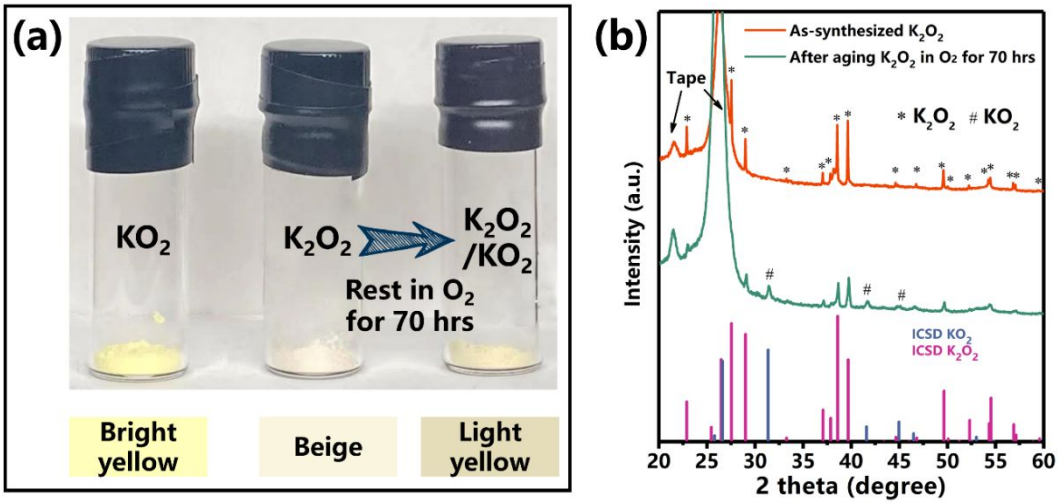

Figure 7. Stability evaluation of K_2O_2 in a pure O_2 atmosphere. (a) Optical images and (b) XRD patterns of K_2O_2 before and after resting in O_2. The optical image of KO_2 powder is added for comparison.

General mind map for realizing the two-electron process in the K-O system

Based on the observation above, some deductions can be obtained as follows.

(1) It is difficult to realize a direct two-electron O_2/K_2O_2 transformation (0 to -2) without involving KO_2 formation because KO_2 is both thermodynamically and kinetically stable at ambient conditions. Notably, dividing into two single-electron processes (0 to -1 and -1 to -2) allows the possibility of realizing the O anionic redox with high reaction kinetics.

(2) K_2O_2 is susceptible to chemical oxidation by O_2. This side reaction consumes the rechargeable K_2O_2 amount and thus affects the redox reversibility ($K_2O_2 \rightarrow KO_2$). In other words, operating in an inert Ar atmosphere is a prerequisite to realize the reversible KO_2/K_2O_2 redox (**Figure 8**a). In addition, the O_2 source that enables O_2/KO_2 redox should come from a condensed O_2 source (e.g., KO_2) rather than gaseous O_2. Only in this situation can the newborn O_2 from KO_2 decomposition be captured and further reduced to KO_2 in the following cathodic scan, which is verified in our designed experiments (**Figure 3** and **Figure 6**).

(3) It is noteworthy to mention the stability differences between alkali metal peroxides. As validated in prior studies, both Li_2O_2[22] and Na_2O_2[24] (thermodynamically stable products) are the possible discharge products in Li-O_2 or Na-O_2 batteries, which is a good implication for the superb stability of Li_2O_2 and Na_2O_2 in the presence of gaseous O_2. Such a deduction is also supported by the evidence that the intermediate LiO_2 and NaO_2 (kinetically stable products) disproportionate spontaneously and yield the corresponding peroxides with gaseous O_2 evolution (**Figure 8**b). In comparison, the KO_2 is the sole stable product in room-temperature K-O_2 batteries.[8] In other words, the disproportionation of KO_2 to K_2O_2 and O_2 is unfavored, and the reverse reaction ($K_2O_2+O_2 \rightarrow 2KO_2$) is favorable. This can also highlight the uniqueness of the K-O system compared to the counterparts of Li-O and Na-O systems.

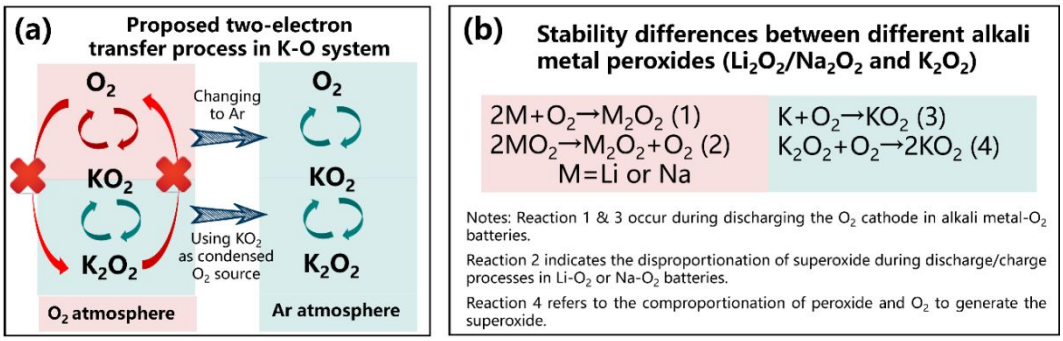

Figure 8. General mind map for realizing the reversible two-electron transfer for O anionic redox without catalysts. (a) Schematically illustration of the proposed two-electron transfer process in the K-O system. (b) Comparison stability differences between alkali metal peroxide.

Perspective

Despite being the youngest metal-O_2 technology, the superoxide-based K-O_2 battery system has established its unrivaled advantage in highly reversible O_2/KO_2 redox, resulting in a high round-trip efficiency without requiring any catalysts. Stabilizing superoxide by the K^+ cation provides the solution to the kinetic challenge in the air cathode and enables investigation of the O-related anionic redox beyond superoxide for practical applications.

Note that a closed cell system with solid KO_2 supply in the absence of O_2 is suggested if we want to achieve high O_2/KO_2/K_2O_2 reversibility in real batteries based on the findings revealed in this manuscript. If we purge the electrolyte with gaseous O_2 priorly, the K_2O_2 formed electrochemically ($KO_2 + e^- + K^+ \rightarrow K_2O_2$) is susceptible to chemical reaction with O_2 by generating KO_2 (Reaction 3) following the ***EC*** mechanism, which reduces the rechargeable K_2O_2 amount and thus affects the reversibility of KO_2/K_2O_2 redox. The alternative option is to choose the condensed O_2 source (e.g., KO_2 or K_2O_2). The relatively strict requirements during K_2O_2 preparation limit its wide use. In comparison, the thermodynamically stable KO_2 can be massively produced, making it suitable for potential large-scale applications. More promisingly, our recent studies show that KO_2 is dry-air stable, which implies its excellent compatibility with dry-room battery manufacturing.[11] Ideally, the KO_2 cathode can couple with a potassium-ion anode to construct a cell that represents the half-discharged state. Nevertheless, the difficulty of preparing the pre-potassiated anodes is a big challenge, and their compatibility with DMSO-based electrolyte also needs further examination, which is subject to further investigation in the future.

Experimental

Materials

Potassium chunks (K, 98.0% purity, Sigma-Aldrich) were stored in the mineral oil. The K surface was cut by a doctor blade and then roll-pressed into foils for further use. Potassium hexafluorophosphate (KPF_6, 99.5%, Sigma-Aldrich), potassium nitrate (KNO_3, 99.0%, Sigma-Aldrich), and potassium superoxide (KO_2, Sigma-Aldrich) were dried in the chemical drier under vacuum before transferring into the glovebox. The dimethyl sulfoxide (DMSO, 99.9%, Sigma-Aldrich) was stored in the bottles with activated 3Å molecular sieves (Sigma-Aldrich) to reduce the water contents below 10 ppm.

Preparation of K_2O_2 and K_2O

Two methods were proposed to synthesize K_2O_2. For **route 1**, it was proposed to wrap

commercial KO_2 powder with the pressed K foil (1:1 by mole) to make a "dumpling". The wrapped "dumpling" was put inside an alumina tube and sealed in an evacuated quartz tube, followed by sintering at 300 ^oC for 12 hours under vacuum and cooling down naturally to room temperature. The heating rate is 5 ^oC/min. For **route 2**, it was advised to weigh the specific amount of K_2O (10% excess in mol) and commercial KO_2 powder. After grinding the mixture thoroughly in the glovebox, a pellet was obtained by pressing the above mixture with a hydraulic machine (400 MPa for 10 mins). The pellet was then sealed in an evacuated quartz tube, steadily heated at a rate of 5 ^oC/min to 300 ^oC, held at this temperature for 12 hours, and naturally cooled down to room temperature. The obtained pellet was re-grinded to powder, and it was advised to repeat the above pressing and sintering procedure to obtain pure K_2O_2.

The synthesis of K_2O was based on our prior study.[30] In general, K_2O was synthesized by wrapping KNO_3 powder with the pressed K foil (5% excess in mol). The mixture was placed on an aluminum boat within a quartz tube under Ar flow, which was then heated at 170 ^oC for 12 hours and naturally cooled down.

Characterization

Powder X-ray diffraction (PXRD) measurements were finished on a Rigaku D/MAX 2500/PC with a Cu Kα source at the step rate of 1.5^o/min. The polymer film (3M) was adhered to the XRD sample holder after heating to protect air-sensitive samples from exposure during tests. Scanning electron microscopy (SEM) images were acquired at an FEI Quanta 200 SEM at an accelerating voltage of 5 kV. The air-sensitive powder sample was transferred into an air-tight holder before observation.

Calibration of Ag/$AgNO_3$ reference electrode ($V_{Ag+/Ag}$) versus $V_{K+/K}$, $V_{Li+/Li}$, and $V_{Na+/Na}$

Ferrocene (Fc, 98%, Sigma-Aldrich) was first added and dispersed into 0.1 M KPF_6/DMSO electrolyte. The Ag^+/Ag reference electrode was calibrated by correlating the known redox potential of Fc/Fc^+ [versus standard hydrogen electrode (SHE)] and the estimated redox potential in 0.1 M KPF_6/DMSO electrolyte. Given the specific voltage gap between SHE and K^+/K, the Ag^+/Ag reference is determined to be 0 $V_{Ag+/Ag}$ ≡ 3.47 $V_{K+/K}$ in the DMSO-based electrolyte. Similarly, the reference potentials of Li^+/Li and Na^+/Na can also be estimated as $V_{Ag+/Ag}$ ≡ 3.65 $V_{Li+/Li}$ and $V_{Ag+/Ag}$ ≡ 3.32 $V_{Na+/Na}$, respectively.

Electrochemical measurements

Three-electrode CV measurements were conducted using an electrochemical workstation (Gamry) and a four-necked, air-tight glass cell. Glassy carbon and platinum wire were employed as the working and counter electrodes. Silver wire in a 0.01 M $AgNO_3$/0.1 M $TBAPF_6$ acetonitrile solution was used as the reference electrode.

The KO_2-saturated electrolyte was prepared as follows: 1) dissolving commercial KO_2 powder in 0.1 M KPF_6/DMSO solution; 2) stirring the above solution overnight in the Ar-filled glovebox; 3) using the filter (pore size 0.45 μm) to filtrate the insoluble KO_2; 4) transferring the clear filtrate for the following tests. Note that the electrolytes were purged with high-purity Ar or O_2 for 10 mins before three-electrode CV measurements.

Author contributions

L. Q.: experimental, validation, formal analysis. writing–original draft; H. A.: experimental, investigation; Y. W.: funding acquisition, supervision, writing–review and editing.

Conflicts of interest

There are no conflicts to declare.

Acknowledgements

This project was financially supported by the Ohio State University and the U.S. Department of Energy (Award No. DE-FG02-07ER46427).

Notes and references

1 J. Y. Cheon, K. Kim, Y. J. Sa, S. H. Sahgong, Y. Hong, J. Woo, S. D. Yim, H. Y. Jeong, Y. Kim and S. H. Joo, *Adv. Energy Mater.*, 2016, **6**, 1–10.
2 C. Xia, C. Y. Kwok and L. F. Nazar, *Science*, 2018, **361**, 777–781.
3 A. Kondori, M. Esmaeilirad, A. M. Harzandi, R. Amine, M. T. Saray, L. Yu, T. Liu, J. Wen, N. Shan, H.-H. Wang, A. T. NGO, P. C. Redfern, C. S. Johnson, K. Amine, R. Shahbazian-Yassar, L. A. Curtiss and M. Asadi, *Science*, 2023, **379**, 499–505.
4 E. Mourad, Y. K. Petit, R. Spezia, A. Samojlov, F. F. Summa, C. Prehal, C. Leypold, N. Mahne, C. Slugovc, O. Fontaine, S. Brutti and S. A. Freunberger, *Energy Environ. Sci.*, 2019, **12**, 2559–2568.
5 P. Hartmann, C. L. Bender, M. Vračar, A. K. Dürr, A. Garsuch, J. Janek and P. Adelhelm, *Nat. Mater.*, 2013, **12**, 228–232.
6 J. Kim, H. Park, B. Lee, W. M. Seong, H. D. Lim, Y. Bae, H. Kim, W. K. Kim, K. H. Ryu and K. Kang, *Nat. Commun.*, 2016, **7**, 1–9.
7 J. Lu, Y. J. Lee, X. Luo, K. C. Lau, M. Asadi, H. H. Wang, S. Brombosz, J. Wen, D. Zhai, Z. Chen, D. J. Miller, Y. S. Jeong, J. B. Park, Z. Z. Fang, B. Kumar, A. Salehi-Khojin, Y. K. Sun, L. A. Curtiss and K. Amine, *Nature*, 2016, **529**, 377–382.
8 N. Xiao, R. T. Rooney, A. A. Gewirth and Y. Wu, *Angew. Chem. Int. Ed.*, 2018, **57**, 1227–1231.
9 X. Ren and Y. Wu, *J. Am. Chem. Soc.*, 2013, **135**, 2923–2926.
10 L. Qin, L. Schkeryantz, J. Zheng, N. Xiao and Y. Wu, *J. Am. Chem. Soc.*, 2020, **142**, 11629-11640.
11 L. Qin, N. Xiao, S. Zhang, X. Chen and Y. Wu, *Angew. Chem. Int. Ed.*, 2020, **59**, 10498-10501.
12 L. Qin, S. Zhang, J. Zheng, Y. Lei, D. Zhai and Y. Wu, *Energy Environ. Sci.*, 2020, **13**, 3656–3662.
13 Z. Zhu, A. Kushima, Z. Yin, L. Qi, K. Amine, J. Lu and J. Li, *Nat. Energy*, 2016, **1**, 16111.
14 Y. Qiao, K. Jiang, H. Deng and H. Zhou, *Nat. Catal.*, 2019, **2**, 1035–1044.
15 J. Wang, R. Gao and X. Liu, *Inorganics*, 2023, **11**, 69.
16 W. Wang, Y. Wang, C. H. Wang, Y. W. Yang and Y. C. Lu, *Energy Storage Mater.*, 2021, **36**, 341–346.
17 Y. Qiao, H. Deng, Z. Chang, X. Cao, H. Yang and H. Zhou, *Natl. Sci. Rev.*, 2021, **8**, nwaa287.
18 L. Qin, S. Luke and Y. Wu, *Angew. Chem. Int. Ed.*, 2023, **62**, e202213996.
19 P. H. Reinsberg, A. Koellisch, P. P. Bawol and H. Baltruschat, *Phys. Chem. Chem. Phys.*, 2019, **21**, 4286–4294.
20 S. Sankarasubramanian and V. Ramani, *J. Phys. Chem. C*, 2018, **122**, 19319–19327.
21 W.-J. Kwak, Rosy, D. Sharon, C. Xia, H. Kim, L. R. Johnson, P. G. Bruce, L. F. Nazar, Y.-K. Sun, A. A. Frimer, M. Noked, S. A. Freunberger and D. Aurbach, *Chem. Rev.*, 2020, **120**,

6626-6683.
22 H. D. Lim, B. Lee, Y. Bae, H. Park, Y. Ko, H. Kim, J. Kim and K. Kang, *Chem. Soc. Rev.*, 2017, **46**, 2873–2888.
23 H. Yadegari and X. Sun, *Acc. Chem. Res.*, 2018, **51**, 1532–1540.
24 C. L. Bender, D. Schröder, R. Pinedo, P. Adelhelm and J. Janek, *Angew. Chem. Int. Ed.*, 2016, **55**, 4640–4649.
25 P. H. Reinsberg, A. Koellisch, P. P. Bawol and H. Baltruschat, *Phys. Chem. Chem. Phys.*, 2019, **21**, 4286-4294.
26 W. Wang, N.-C. Lai, Z. Liang, Y. Wang and Y.-C. Lu, *Angew. Chem. Int. Ed.*, 2018, **57**, 5042-5046.
27 Ralph G. Pearson, *J. Am. Chem. Soc.*, 1963, **85**, 3533–3539.
28 O. Gerbig, *Thesis*, 2014.
29 C. Freysoldt, P. Merz, M. Schmidt, S. Mohitkar, C. Felser, J. Neugebauer and M. Jansen, *Angew. Chem. Int. Ed.*, 2019, **58**, 149–153.
30 J. Zheng, H. Fang, L. Fan, Y. Ren, P. Jena and Y. Wu, *J. Phys. Chem. Lett.*, 2021, **12**, 7120–7126.